JCTC Journal of Chemical Theory and Computation

Article

pubs.acs.org/JCTC

Divalent Ion Dependent Conformational Changes in an RNA Stem-Loop Observed by Molecular Dynamics

Christina Bergonzo,[†] Kathleen B. Hall,[‡] and Thomas E. Cheatham, III*[,†]

[†]Department of Medicinal Chemistry, College of Pharmacy, University of Utah, Salt Lake City, Utah 84112, United States

[‡]Department of Biochemistry and Molecular Biophysics, Washington University School of Medicine, St. Louis, Missouri 63110, United States

Supporting Information

ABSTRACT: We compare the performance of five magnesium (Mg^{2+}) ion models in simulations of an RNA stem loop which has an experimentally determined divalent ion dependent conformational shift. We show that despite their differences in parametrization and resulting van der Waals terms, including differences in the functional form of the nonbonded potential, when the RNA adopts its folded conformation, all models behave similarly across ten independent microsecond length simulations with each ion model. However, when the entire structure ensemble is accounted for, chelation of Mg^{2+} to RNA is seen in three of the five models, most egregiously and likely artifactual in simulations using a 12-6-4 model for the Lennard-Jones potential. Despite the simple nature of the fixed point-charge and van der Waals sphere models employed, and with the exception of the likely oversampled directed chelation of the 12-6-4 potential models, RNA−Mg^{2+} interactions via first shell water molecules are surprisingly well described by modern parameters, allowing us to observe the spontaneous conformational shift from Mg^{2+} free RNA to Mg^{2+} associated RNA structure in unrestrained molecular dynamics simulations.

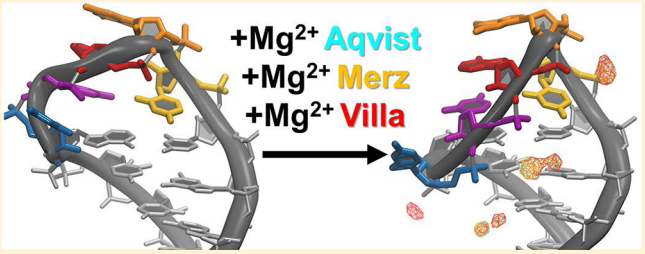

INTRODUCTION

Simulating a heterogeneous solvent environment, which is especially important for RNA, adds complexity to simulations. Intramolecular interactions between dynamic RNA secondary structure and tertiary structure elements are typically dependent on solution conditions for their formation and stability.[1] Most commonly, divalent Mg^{2+} ions are required for these structures to form, either to effectively shield the high charge density of proximal phosphates or to facilitate or stabilize a conformation required for the interaction.[2] Both secondary structure elements and tertiary structure contacts can be strongly stabilized by Mg^{2+}.[1,2]

Traditionally, simulations have had trouble describing the highly polarizable nature of divalent ions, which is not explicitly captured in a classical, fixed charge model.[3,4] Polarizable force fields have shown mixed results for the parametrization of nucleic acids,[5] though recent parameters using Drude oscillator approaches to address the balance between nucleic acids, monovalent ions, and solvent have shown improved results.[6,7] Mg^{2+} ions and their solution effects have been approximated using many methods, including continuum methods,[8,9] reduced models, and multisite models. Reduced models have been shown to reproduce both the diffuse and chelated/associated ion effects when combined with explicit Mg^{2+}.[10,11] Multisite models, which shift partial charges onto external sites, have also been used to capture the interactions of associated Mg^{2+} ions with nucleic acids.[12,13] Though all of these models can reproduce various types of experimental data, a more fully applicable point-charge model requires the ability to capture the dynamics of chelated, associated, and also bulk Mg^{2+} effects.

Recently, four reparametrizations for fixed charge Mg^{2+} have been released. In the Allner et al. modifications, Mg^{2+} parameters are optimized to fit the experimental exchange rate of the first shell water molecules by modifying the repulsive Lennard-Jones (LJ) term (Villa).[14] The Li et al. 12-6 modifications are fit to the experimental hydration free energies and the ion−oxygen distance, and then are combined into a consensus set (Merz).[15] Though parametrized independently, the resulting Villa and Merz 12-6 LJ parameters are somewhat similar, increasing the distance of the minimum (Rmin) and making the well depth (epsilon) more shallow compared to the widely used Aqvist parameters (Table 1).[16] Li and Merz also developed a divalent model based on a 12-6-4 LJ functional, adding a $1/r^4$ term to capture charge induced dipole effects (12-6-4).[17] Panteva et al. found that these parameters resulted in an overestimation of the binding free energy of Mg^{2+} to nonbridging phosphate oxygen atoms and an underestimation of the binding free energy of Mg^{2+} to the N7 atom of adenosine and guanine bases.[18,19] They developed modified 12-6-4 parameters (m12-6-4) which apply different polarizabilities

Received: February 15, 2016
Published: June 13, 2016

DOI: 10.1021/acs.jctc.6b00173
J. Chem. Theory Comput. 2016, 12, 3382−3389

Table 1. Mg^{2+} Ion Lennard-Jones Parameters Tested in This Work

	$R_{min}/2$ (Å)	ε (kcal/mol)	C12	C6	C4[a]
Aqvist	0.7926	0.8947	225	28.4	n/a
Merz	1.360	0.01020237	1673	8.26	n/a
Villa	1.5545	0.00295	2400	5.32	n/a
12-6-4/m12-6-4	1.437	0.02258	7171	25.4	4.42

[a]n/a = not applicable.

for these atom types, tuning the interactions to experimental site specific binding free energies.[19]

Following the procedure of Joung and Cheatham, each of the preceding different ion parameter sets was generated for use with specific water models.[20] In the 12-6-4 models, this is achieved by scaling the C4 terms of each atom type by the ion−water oxygen atom interaction (C4(H_2O)) and the polarizability of the specific water model, as follows:

$$\mathrm{C4(atom\ type)} = \frac{\mathrm{C4}(H_2O)}{\alpha_0(H_2O)}\alpha_0(\mathrm{atom\ type}) \quad (1)$$

For the simulations in this work, the C4 for Mg^{2+} in TIP3P water is 132.9 Å^4·(kcal/mol).[17]

The LJ parameters for Mg^{2+} models used in this work, and their calculated self C12, C6, and C4 interactions, are reproduced in Table 1. A more detailed table with the LJ matrix calculated for the 12-6-4 and m12-6-4 Mg^{2+} ion interactions with all atom types, showing Rmin, epsilon, and C12, C6, and C4 coefficients, is given in Supporting Information Tables S1 and S2.

The dynamics and structure of the Varkud satellite ribozyme stem-loop V RNA (SLV) have been shown experimentally to be Mg^{2+} ion dependent.[21,22] In the absence of Mg^{2+}, the five nucleotide U-turn loop exhibits considerable dynamics and adopts a wide range of structures.[21,23] When Mg^{2+} is present, the loop is stabilized in a canonical U-turn conformation byMg^{2+} ions, as shown in Figure 1.[22] The goal of this work is to determine whether Mg^{2+} ion models can accurately describe the dynamic structure shift from a magnesium free (MgFree) conformation to the magnesium bound (MgBound) conformation. Using molecular dynamics simulations, we examine the differences between ion models after the RNA has transitioned to the MgBound form and then for all conformations sampled in the simulations. By using 10 sets of independent 1−1.5 μs MD simulations with varying starting ion positions for each Mg^{2+} ion parameter set, we compare ion binding for the five models. We find that all models promote the MgFree to MgBound transition in SLV RNA. Both sets of 12-6-4 potential Mg^{2+} ions trend toward more occupied interactions due to loss of inner shell water molecules in all simulations, while the Villa Mg^{2+} ions lost inner shell water molecules in several simulations. Interestingly, the Merz and Aqvist Mg^{2+} ions give remarkably similar results as far as occupancies in the folded state and the ensemble of folded and unfolded structures, despite their differing LJ parameters. For future simulations of SLV RNA, Merz 12-6 Mg^{2+} ions will be used, but more validation against experimental observables for other RNA systems should be performed.

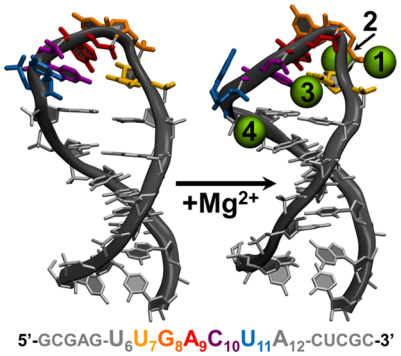

Figure 1. SLV RNA in the absence and presence of Mg^{2+}. SLV RNA in the absence of Mg^{2+} adopts a loose U-turn structure (left; PDB ID, 1TBK), which shifts conformation to a canonical U-turn structure upon Mg^{2+} binding (right; PDB ID, 1YN2). The positions of the Mg^{2+} ions are based on NMR experiments and are labeled 1−4.[22] The SLV sequence and numbering used in our simulations are shown at the bottom of the image. The hairpin loop is formed by the U6:A12 noncanonical loop-closing base pair, with U7-G8-A9-C10 forming a U-turn, extruding U11. Experimentally determined hexahydrated Mn^{2+} binding sites are shown as green spheres, numbered 1−4.

MATERIAL AND METHODS

The coordinates of MgFree SLV RNA were taken from the first model (labeled as the best representative conformer) in the 1TBK NMR ensemble.[21] The RNA was neutralized with 8 Mg^{2+} ions and solvated with 3967 TIP3P water molecules.[24] An additional four Mg^{2+} ions, five K^+ ions, and 13 Cl^- ions were added to generate approximately 40 mM $MgCl_2$ and 50 mM KCl concentrations. Systems were built five times, using Aqvist ion parameters to generate the "Aqvist" set,[16] Li et al. consensus set parameters to generate the "Merz" set,[15] Allner et al. parameters to generate the "Villa" set,[14] Li and Merz 12-6-4 parameters to generate the "12-6-4" set,[17] and Panteva et al. m12-6-4 parameters to generate the "m12-6-4" set.[19] AMBER formatted prepin and frcmod files are included in the Supporting Information for using these parameters in Amber14 (Files S1−S4). Additionally, the *add12_6_4* command in parmed.py was used to generate an AMBER parmtop with the additional C4 terms for the 12-6-4 potential simulations. Parmed.py was also used to create new atom types for the N7 atoms of adenosine and guanosine (ND and NG, respectively) and the nonbridging phosphate oxygen atoms (O2) for the m12-6-4 model. Initial ion positions were randomized 6.0 Å from the RNA solute and 4.0 Å from each other, using 10 different seeds for each model. This resulted in 10 starting structures with randomized ion environments for each ion model tested.

Simulations for the 12-6 potential systems (Aqvist, Merz, and Villa) were carried out using the Amber14 suite of programs GPU (CUDA) version of PMEMD with SPFP (a mixed single/fixed precision model on the GPU).[25,26] Simulations for the 12-6-4 potential systems were performed using the Amber14 CPU version of PMEMD, with the lj1264 = 1 flag set in the input. The ff12 force field for nucleic acid simulations was used, combining ff99[27] + parmbsc0 modifications[28] + chiOL3 modifications[29] for RNA. The particle mesh Ewald method, with default parameters, was used to handle electrostatic interactions with a 9 Å cutoff for direct interactions.[30] Bonds to hydrogen were constrained using the SHAKE algorithm, allowing use of a 2 fs time step.[31] Hydrogen mass repartitioning was employed for the 12-6-4 potential simulations performed on the CPU, allowing a 4 fs time step.[32] For these simulations the masses of atoms bonded to hydrogen were decreased by

DOI: 10.1021/acs.jctc.6b00173
J. Chem. Theory Comput. 2016, 12, 3382−3389

3.024 Da using parmed.py, and the hydrogens' mass was increased by the same amount.

Each of the 50 total systems was minimized with 500 steps steepest descent and 500 steps conjugant gradient with 25 kcal mol^{-1} restraints on the RNA, followed by heating to 300 K over 100 ps, maintaining constant volume. Temperature was regulated using the weak-coupling algorithm, and a coupling time constant of 0.2 ps was used.[33] The translational center of mass motion was removed every 10 ps. After heating, each system was subjected to rounds of 500 steps steepest descent, 500 steps conjugate gradient minimization, and 50 ps constant pressure equilibration with decreasing positional restraint weights (5.0, 4.0, 3.0, 2.0, and 1.0 kcal mol^{-1}). During these rounds of constant pressure equilibration, the pressure relaxation time was set to 2 ps. A final equilibration was run for 500 ps at constant pressure with 0.5 kcal mol^{-1} restraints, after which restraints were removed and a 50 ps unrestrained constant pressure simulation was run, with temperature coupling time constant set to 5 ps and the pressure relaxation time set to 5 ps.

Production runs began for each ion set from the 10 equilibrated systems, and the properties of the RNA and ions were measured from this portion of the trajectory. Production runs were constant volume and temperature. Temperature was set to 300 K and regulated using the Langevin algorithm with a collision frequency of 5 ps^{-1} and random seeds used for initial velocity assignments, preventing synchronization artifacts.[34,35]

Analysis was performed using CPPTRAJ[36] and visualized in VMD.[37] H-bond analysis was performed using a distance cutoff of 4.0 Å between Mg^{2+} ions and all atoms of the RNA. All folded RNA structures from all ion model runs using either a 12-6 LJ potential or a 12-6-4 LJ potential were used to generate an average structure for grid analysis. Grids were normalized to a Mg^{2+} ion density of 9.7×10^{-5} mol/Å^3. Results were plotted using Grace or Microsoft Excel.

RESULTS

Mg^{2+} Ion Models Shift VSR RNA from the Unbound Conformation to the Bound Conformation. Previous simulations were performed on SLV RNA, starting from the MgBound and MgFree forms, in the presence of either 50 mM NaCl or 40 mM $MgCl_2$.[23] These simulations showed that when monovalent ions are present, the SLV RNA folds to a MgBound-like structure with an RMSD of ~2.0 Å from the MgBound loop structure, irrespective of the starting conformation. We denoted this "gatekeeper" structure as a precursor to Mg^{2+} ion binding, upon which the RMSD to the MgBound loop shifts to a lower 1.625 Å value and the U-turn motif is stabilized via Mg^{2+} ion association. The lower RMSD structure (the "folded" loop) is not observed in simulations with monovalent salt, either in short simulations (hundreds of nanoseconds) or during replica exchange simulations (57.6 μs of aggregate simulation time).[23] In the presence of divalent ions, the SLV RNA sampled low RMSDs to the MgBound reference in the simulations starting from either MgBound or MgFree structures. Even in short hundred nanosecond time scale simulations, the MgFree loop folded to the MgBound state upon the addition of $MgCl_2$. In an effort to better understand the role of Mg^{2+} in loop folding, we have extended this simulation set in the current work.

Ten copies of the equilibrated system, where the Mg^{2+} ions added were parameters from Aqvist,[16] Merz,[15] Villa,[14] 12-6-4,[17] or m12-6-4,[19] were each run for 1−1.5 μs. The addition of Mg^{2+} ions to the system should result in a switch from the MgFree RNA structure to the MgBound RNA structure. Figure 2 shows the histogram of loop RMSD to the folded MgBound

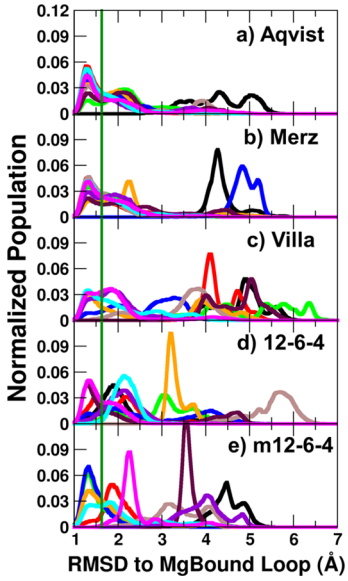

Figure 2. Histograms of the RMSD of SLV RNA loop atoms to the "folded" MgBound structure for each of 10 simulations containingthe following: (a) Aqvist Mg^{2+} ions, (b) Merz Mg^{2+} ions, (c) Villa Mg^{2+} ions, (d) 12-6-4 Mg^{2+} ions, and (e) m12-6-4 Mg^{2+} ions. Time dependent data with 1000 step running averages are shown in Supporting Information Figure S1. In all plots, the green line represents the 1.625 Å cutoff below which structures are considered "folded" or MgBound.

structure and shows that very low RMSDs are achieved in simulations performed in each ion model. Simulations sample structures which are considered folded (those below the green line indicating an RMSD of 1.625 Å) in the presence of all Mg^{2+} ion models. The MgBound structure is sampled in 9/10 Aqvist simulations, 8/10 Merz simulations, 6/10 Villa simulations, 8/10 12-6-4 simulations, and 8/10 m12-6-4 simulations. Although not all of the structures have converted to the MgBound structure in the 1−1.5 μs of MD simulation time, the majority of simulations in each case have transitioned. Given this, the simulations were not extended further; although longer simulations may show transitioning of all structures, full convergence of the structural distributions would likely require application of enhanced sampling methods, such as replica exchange.[38−40]

Mg^{2+} Ion Models Show Similar Association with RNA in the Bound Conformation. To understand the influence of each ion model on the bound structure, we first combined all structures (for 10 simulations using each ion model) below a cutoff of 1.625 Å RMSD to the MgBound loop, described previously as the cutoff between gatekeeper and MgBound (or folded) structures.[23] The low RMSD-to-MgBound structures were analyzed using the hbond command in CPPTRAJ to determine the fraction occupancies of Mg^{2+} ions to all RNA atoms. Average structures were generated from the three 12-6 LJ parameter models, Aqvist, Merz, and Villa, and from the 12-6-4 LJ potential models, 12-6-4 and m12-6-4, and Mg^{2+} ion occupancies were mapped onto them.

When the RNA is folded in the same conformation, the 12-6 potential ion models generally behave in the same manner. The

DOI: 10.1021/acs.jctc.6b00173
J. Chem. Theory Comput. 2016, 12, 3382−3389

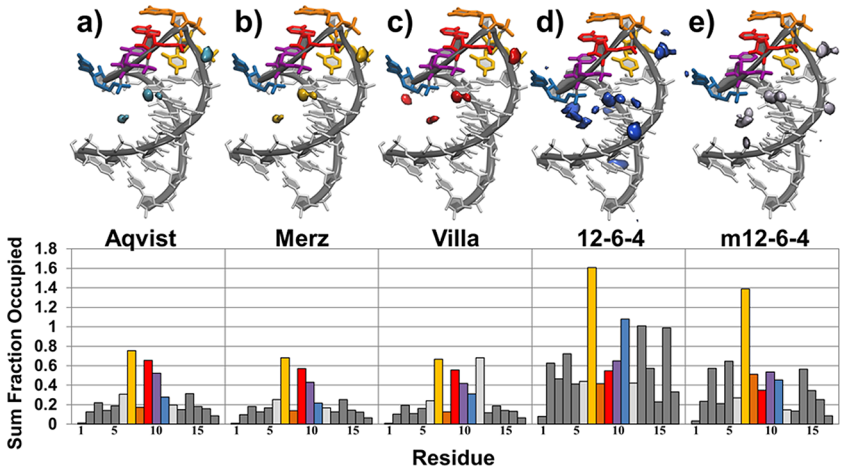

Figure 3. Top: Mg^{2+} ion density grids at >10% occupancy (250−500× bulk occupancy) for SLV RNA atoms for each ion model: (a) Aqvist, (b) Merz, (c) Villa, (d) 12-6-4, and (e) m12-6-4. Bottom: Sum of fraction occupancies for all residues (1−17) for all systems (Aqvist, Merz, Villa, 12-6-4, and m12-6-4), where stem residues 1−5 and 13−17 are shown in dark gray, loop-closing base pair residues 6 and 12 are shown in light gray, and loop residues 7−11 are colored to match the bases in Figure 1 and panel a.

similarity of these interactions can be seen in Figure 3a−c, which shows the average folded MgBound structure and localized Mg^{2+} densities (500× greater than bulk Mg^{2+} ion densities, or 10% occupancy from hbond). The sum of occupancies for the atoms in each residue of SLV RNA (1−17) are shown below the SLV RNA for each ion model. The profiles reinforce the similarity between the 12-6 models, especially the Aqvist and Merz models. In general, the highest occupancies center on phosphate oxygen atoms. Specifically, the U-turn nucleotides U7-G8-A9 coordinate a Mg^{2+} ion, locking in the folded structure, differentiating the folded structure from the rest of the ensemble. Another area of high Mg^{2+} ion density is between C10 and U11 phosphate oxygen atoms. Mg^{2+} ions can be seen associating with RNA atoms in the major groove and at phosphate oxygen atoms when interactions populated at 10% occupancy are considered (Figure S2).

An interesting difference between ion models' association with the MgBound RNA is the high occupancy in the 12-6-4 LJ potential models, shown in Figure 3d,e. Though the occupancy is mapped onto SLV RNA at the same 500× bulk concentration as the 12-6 models, there are many more highly occupied sites. The sum of the fraction occupancies per residue shown below the SLV RNA reinforces that there is, in general, more highly occupied sites than the 12−6 models. This is due to the Mg^{2+} ions described by the 12-6-4 parameters and, to a lesser extent, the m12-6-4 parameters losing an inner shell water molecule and forming a chelated interaction with the RNA, but there is no obvious structural explanation for this chelation.

Sites for Mg^{2+} ion association have been experimentally determined by NMR chemical shift perturbation using manganese hexahydrate and cobalt hexammine[22] and are mapped onto the SLV structure in Figure 1. Those experiments could not determine fractional occupancy or residence time for the ions. Simulations provide those parameters for each Mg^{2+} ion association site, and Table 2 shows the results for each ion model. The results show the distribution of interactions across the RNA atoms is almost identical for each ion model which uses a 12-6 LJ potential. The trend for more and less occupied binding site interactions holds for the 12-6-4 LJ potential models, but overall the occupancies are higher. The models agree in the lack of Mg^{2+} occupying site 2. This site was

Table 2. Percent Occupancy for Mg^{2+} Atoms in Experimentally Determined RNA Binding Sites, Calculated for Folded Structures[a]

		folded cluster, Mg^{2+} (%)				
binding site	atom	Aqvist	Merz	Villa	12-6-4	m12-6-4
1	U_7@OP1	3.15	2.75	2.54	32.88	11.55
	U_7@OP2	62.8	58.07	55.52	76.85	79.15
	U_7@O5′	0	0	n.f.	36	29.87
	G_8@OP1	5.94	4.93	4.5	15.53	28.82
	G_8@O3′	0.02	0.02	0.35	3.22	0.04
	A_9@OP1	11.95	10.41	10.32	19.38	6.74
	A_9@OP2	53.04	46.21	42.78	26.64	26.72
2	U_7@O2′	0.1	0.07	0.05	0.26	0.3
	G_8@N7	1.06	0.85	0.67	2.42	3.97
	A_9@N7	0	n.f.	n.f.	n.f.	0
3	U_6@O4	24.75	20.08	19.58	21.67	20.42
	U_7@O4	8.07	6.38	7.88	10.14	9.97
	C_10@OP1	19.53	16.51	17.54	17	13.01
	C_10@OP2	31	24.95	23.04	23.41	29.44
4	U_11@OP1	10.26	8.86	10.03	67.58	27.94
	U_11@O3′	0.08	0.05	8.31	3.54	0.87
	A_12@N7	0	n.f.	0	n.f.	n.f.

[a]n.f. = not found.

determined based on $Mn(H_2O)_6^{2+}$ proximity to the RNA, which could have formed d-orbital interactions with site 2 atoms, accounting for the discrepancy between simulation and experiment. However, the m12-6-4 simulations, which explicitly address the balance between Mg^{2+} interactions with N7 atoms, have a higher occupancy of G8@N7, indicating a deficit in the 12-6 LJ potential models. Additionally, in the 12-6 LJ potential simulations, K^+ ions have a higher occupancy than Mg^{2+} for site 2 atoms, shown in Table S3.

Combined Data Indicate Subtle Differences between Models. Figure 4 shows the aggregate data for all 10 simulations performed for each ion model, separated into interactions between Mg^{2+} and phosphate oxygen atoms, base oxygen and nitrogen atoms, and sugar oxygen atoms. It is apparent that each ion model prefers associated interactions with phosphate oxygen atoms, since these interactions range

DOI: 10.1021/acs.jctc.6b00173
J. Chem. Theory Comput. 2016, 12, 3382−3389

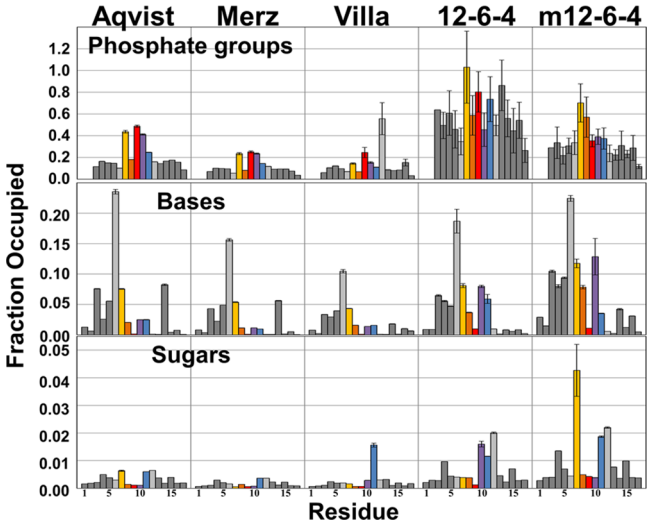

Figure 4. Fraction occupancies by residue (1−17) for Mg^{2+} to RNA interactions for all Mg^{2+} ion models (left to right: Aqvist, Merz, Villa, 12-6-4, and m12-6-4). Top: Phosphate atom interactions (including O3′, O5′, OP1, and OP2). Middle: Base atom interactions (including N9, N7, O6, N1, N2, N3, N4, O2, N6, and O4). Bottom: Sugar atom interactions (including O4′ and O2′). Stem residues 1−5 and 13−17 are shown in dark gray, loop-closing base pair residues 6 and 12 are shown in light gray, and loop residues 7−11 are colored to match the bases in Figures 1 and 3a.

from 10 to 70% occupied. The highest occupancy sites in all 12-6 potential models are in the five residue loop or its closing base pair, where the phosphate backbone populates an unusual conformation involving residues U7 and A9. The 12-6-4 simulations show very high occupancies for phosphate interactions, indiscriminately interacting with SLV RNA throughout the combined data set, instead of showing specific localization in the U-turn region. This effect is reduced when the m12-6-4 LJ potential is used, but the resulting occupancies for the m12-6-4 model are not as low as in the 12-6 models.

Interactions with base atoms range from 0 to 25% occupancy, with the most occupied interaction occurring with the U6 base O4 atom in all ion models. U6:A12 is a noncanonical loop-closing base pair, and the U6@O4 atom could be associated with an Mg^{2+} ion. This agrees with the experimental observation that this base pair is transiently formed based on the very weak experimental NOE in the presence of Mg^{2+}. The increased occupancy for base atoms in the 12-6-4 model, and particularly in the m12-6-4 model, arises from interactions with the N7 atoms of the adenosine and guanosine bases in the loop (residues G8 and A9) and indicates that the polarizability introduced by the 12-6-4 model, and its subsequent tuning in the m12-6-4 model, is important to adequately describe these interactions.

The sugar atoms show very low occupancy, typically less than 2% for all models. The outlier occupancy of residue U7 in the m12-6-4 model arises due to the proximity of Mg^{2+} interacting with the OP1 phosphate of its neighboring residue G8. It is interesting to note that the 12-6-4 LJ parameter models trend toward higher occupancies for all interaction types, and though this effect is ameliorated by using the m12-6-4 corrections, those occupancies are still higher than the 12−6 potential models.

The high occupancies for the 12-6-4 LJ potential models, and their larger error bars, result from chelated interactions with the RNA atoms. Direct chelation involves the hexahydrated Mg^{2+} ion losing an inner shell water molecule in favor of binding to an RNA atom, and these events are summarized in Table 3.

Table 3. Summary of Mg^{2+} Ion Chelation Events[a]

ion model	no. of simulations with a chelation event	av no. of chelating Mg^{2+} (out of 12 total Mg^{2+} ions)	av occupancy of chelating Mg^{2+}
Aqvist	0	n.f.	n/a
Merz	0	n.f.	n/a
Villa	6	0.8 ± 0.8	0.70 ± 0.20
12-6-4	10	7.8 ± 1.6	0.72 ± 0.24
m12-6-4	10	3.9 ± 1.8	0.65 ± 0.27

[a]n.f. = not found; n/a = not available.

The Villa simulations are the only 12-6 potential model where chelation is observed, indicated by the high occupancy or high variability in the phosphate interaction with residues A9, A12, and G16 in Figure 4. A single simulation shows a chelated interaction between an Mg^{2+} ion and the OP1 atom of residues A9 and G16. Half of the simulations contain a chelated interaction between an Mg^{2+} and OP1 of residue A12. In all 10 simulations using both the 12-6-4 and m12-6-4 LJ parameters an Mg^{2+} ion loses an inner shell water molecule to form at least one chelated interaction to a phosphate oxygen atom. Every residue's phosphate group forms a chelated interaction with the 12-6-4 and m12-6-4 Mg^{2+} ions during the combined set of simulations. On average, eight Mg^{2+} ions are chelated to RNA atoms during a simulation with 12-6-4 LJ parameters, and this effect is decreased to four chelated Mg^{2+} ions during a simulation using the m12-6-4 LJ parameters.

When the RNA has already folded to the MgBound structure, the chelating ion has no effect on the RNA, as shown in Figure 5a. However, in some cases the chelation

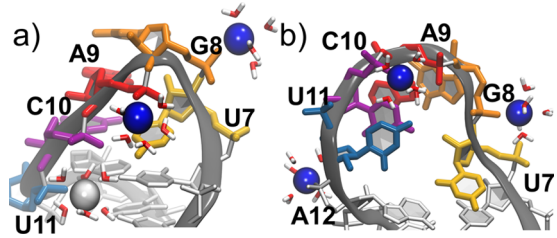

Figure 5. Mg^{2+} ion chelation effects in 12-6-4 simulations. (a) Ion chelation (blue) to G8 phosphate after SLV RNA loop folding does not disrupt the folded loop structure or association of other ions (silver). (b) Ion chelation (blue) to the same G8 phosphate oxygen disrupts the phosphate backbone, and loop folding does not occur.

occurs before the loop folds to the MgBound structure, and the Mg^{2+}−RNA interaction locks the loop backbone conformation, prohibiting reorganization to the correct U-turn fold, depicted in Figure 5b. Once directly chelated with RNA, it would be difficult on these time scales to see the loss of this interaction, and we do not; as with the expected direct chelation binding affinity, likely simulations on the order of 10s of milliseconds would be required to see exchange. These long residence times are reflected in the high occupancies of the chelated interactions which are shown in Table 3. Neither the Aqvist nor Merz models' Mg^{2+} ions lose an inner shell water molecule in favor of directly chelating an RNA atom, though this may be an issue of simulation length. A complete list of chelated Mg^{2+}−

DOI: 10.1021/acs.jctc.6b00173
J. Chem. Theory Comput. 2016, 12, 3382−3389

RNA interactions, separated by ion model, simulation, and atom, is shown in Table S4.

DISCUSSION

In our previous work we looked at the dynamics of SLV RNA, which has been experimentally shown to adopt a Mg^{2+} dependent U-turn structure. Our re-refinement and solution state simulations of the MgFree loop showed that, in the presence of monovalent ions, the SLV RNA adopts a fold that is similar to the MgBound loop. However, the MgFree conformation is distinct in a number of important ways—when Mg^{2+} is present, the loop becomes more compact, stabilizing SLV as a scaffold for substrate binding and neutralizing the charges of the U-turn region to promote binding. As a proof of concept to show the structure is dependent on the ion environment, we ran short simulations (hundreds of nanoseconds in length) to show that the MgBound structure is only adopted in divalent salt.

In this work, we extended the simulations of the MgFree loop in the presence of Mg^{2+} ions and compare the effectiveness of the Aqvist,[16] Merz,[15] and Villa[14] 12-6 potential Mg^{2+} ion models, the Li 12-6-4 potential Mg^{2+} ion model,[17] and the Panteva et al. modifications to the 12-6-4 potential model[19] in reproducing the conformational change of SLV RNA from MgFree to MgBound. All five models induce the conformational change, to some extent, shown by low RMSDs to the MgBound NMR structure in Figure 2, as well as time dependent RMSD from the MgBound NMR structure in Figure S1. Though we cannot converge the RNA structure distribution on this time scale, we can look at the effect of the ions on RNA structure over the ensemble of structures generated in the same amount of simulation time, as well as structures which have transitioned to the "folded" or MgBound conformation. For the folded SLV RNA, this yielded at least 175 K individual frames per ion model, and in some cases 500 K frames, i.e., a non-negligible number of structures.

When the RNA adopts the same conformation, specifically a loop RMSD to the MgBound reference lower than a 1.625 Å cutoff, the Mg^{2+} ions associate with MgBound RNA in almost identical sites in all models. The most similar are the Aqvist and Merz models, which show Mg^{2+} ion association in three out of the four previously described binding sites. The subtle difference between these two models can be seen in the fraction occupancies reported in Table 2, with Aqvist ions trending toward higher fractions of occupied interactions. The Villa Mg^{2+} ion model follows the same trend in occupancies for the folded SLV RNA, with the exception that direct chelation occurs between Mg^{2+} and the 3′ phosphate group of residue 12, leading to seemingly artificial high occupancy for this region. Both the 12-6-4 and m12-6-4 models, which use an additional C4 potential term to approximate the effect of polarizability, have higher occupancies in general when compared to the 12-6 LJ potential models. The overestimation in the binding free energy of Mg^{2+} to RNA phosphate nonbridging oxygen atoms was noted previously,[18] and corrected in the m12-6-4 model.[19] Though the occupancies are lowered in the m12-6-4 simulations compared to the 12-6-4 model, they remain higher than the 12−6 LJ potential models. Overall, when SLV RNA is in its folded conformation, binding sites 1, 3, and 4 show consistent occupancy in all ion models, while binding site 2 shows systematically lower, but nonzero, occupancy.

Differences between models arise when all data across the 10 simulations performed for each model are considered. Figure 4 shows the fraction occupancies for Mg^{2+} associating with phosphate, base, or sugar atoms. The models trend toward the 12-6-4 having the highest occupancies, followed by m12-6-4, Aqvist, Mer,z and Villa. The exception to this trend can be seen in specific interactions where Villa, 12-6-4, and m12-6-4 ions have directly chelated to the RNA. This happens at three atoms with the Villa parameters, but at many more RNA atoms in the 12-6-4 potential simulations—in fact, when the entire set of 12-6-4 simulations is considered, there is not a single phosphate group where chelation does not occur. The implications of chelating ions can be seen in Figure 5. If an ion chelates after the loop is folded, it does not necessarily alter the conformation (Figure 5a). However, ion chelation can prohibit folding to the correct structure by trapping phosphates in alternate backbone conformations precluding ion association in the experimentally determined sites (Figure 5b). It could be bad luck that we see direct chelation in the Villa simulations, and if all 12-6 LJ potential simulations were extended, we would see it occur in other ion models, too. However, on this time scale, neither the Aqvist nor Merz models Mg^{2+} lose an inner shell water molecule. The chelation effect in the 12-6-4 LJ potential simulations is comprehensive.

The simulations performed in this study aggregate 15 μs for each ion model and converge the Mg^{2+} ion distribution when there is only association of Mg^{2+} ions with SLV RNA binding sites (Figure S3). This time scale was expected based on experimental evidence of associating ions.[22] The convergence of the Mg^{2+} ion distribution when those ions chelate directly to RNA would take simulations on the order of 10s of milliseconds to observe multiple binding and unbinding events for Mg^{2+} ions to overcome 12−13.5 kcal/mol free energy barriers to desolvation,[14,19] and are fairly prohibitive. This is reflected in the disagreement of occupancies for binding sites when all simulation data are considered (Table S5). Additionally, we do not converge the RNA distribution. The structures where Mg^{2+} is not associated with RNA vary between models and are not dependent on the ion models themselves (Figure S4). Where Mg^{2+} is chelated to RNA atoms, some simulations become trapped in structures which are artificially stabilized by the chelating ion. This means that the observation that different numbers of simulations sample the MgBound state is not necessarily related to the ion model used in those simulations. Since this work has shown the time dependent folding of SLV RNA, an enhanced sampling technique might be useful to converge the SLV RNA structure distribution when Mg^{2+} ions are present.

CONCLUSIONS

The objective of this study was to reproduce the Mg^{2+} ion dependent conformational change for VSR SLV RNA, from the MgFree to MgBound loop. We tested five Mg^{2+} ion parameters which used two different functional forms of the LJ potential. The 12-6 LJ potential was tested with the widely used Aqvist parameters, and the more recent Merz and Villa modifications. The 12-6-4 potential Li parameters, and their modifications to balance interactions between Mg^{2+} and RNA, were also tested. With all five models, we observed switching from the MgFree RNA to the MgBound RNA structure. The Mg^{2+} ions consistently associated with common sites in the folded SLV RNA and agreed with experimental data. The extent of folding differed between ion models and is likely a time scale issue. However, chelated interactions interfered with folding in the 12-6-4 LJ potential simulations with both the 12-6-4 and m12-

DOI: 10.1021/acs.jctc.6b00173
J. Chem. Theory Comput. 2016, 12, 3382−3389

6-4 models, and to a lesser extent in the 12-6 LJ potential Villa simulations. In the combined data set, where MgFree and MgBound structures were present, the 12-6-4 ions had the highest fraction occupancies overall. Of the 12−6 potential models, the Aqvist ions had higher fraction occupancies, followed by Merz and then Villa, following the trends in increasing van der Waals radii and reduced well depth.

■ ASSOCIATED CONTENT

Supporting Information

The Supporting Information is available free of charge on the ACS Publications website at DOI: 10.1021/acs.jctc.6b00173.

Additional figures, tables, and AMBER compatible force field files for each ion model (PDF)

■ AUTHOR INFORMATION

Corresponding Author

*Tel.: 1 (801) 587-9652. E-mail: tec3@utah.edu.

Funding

This work was supported by the National Institutes of Health (Grant R01-GM098102). This research was enabled by the Blue Waters sustained-petascale computing project (Grants NSF OCI 07-25070 and PRAC OCI-1515572), the National Science Foundation Extreme Science and Engineering Discovery Environment (XSEDE, Grant OCI-1053575 and Allocation MCA01S027P), and the Center for High Performance Computing at the University of Utah.

Notes

The authors declare no competing financial interest.

■ REFERENCES

(1) Qiu, H.; Kaluarachchi, K.; Du, Z.; Hoffman, D. W.; Giedroc, D. P. Thermodynamics of Folding of the RNA Pseudoknot of the T4 Gene 32 Autoregulatory Messenger RNA. *Biochemistry* **1996**, *35*, 4176−4186.

(2) Laing, L. G.; Gluick, T. C.; Draper, D. E. Stabilization of RNA Structure by Mg Ions. Specific and Non-Specific Effects. *J. Mol. Biol.* **1994**, *237*, 577−587.

(3) Stafford, K. A.; Palmer, A. G., III. Evidence from Molecular Dynamics Simulations of Conformational Preorganization in the Ribonuclease H Active Site. *F1000Research* **2014**, *3*, 67−75.

(4) Mamatkulov, S.; Fyta, M.; Netz, R. R. Force Fields for Divalent Cations Based on Single-Ion and Ion-Pair Properties. *J. Chem. Phys.* **2013**, *138*, 024505-1−024505-12.

(5) Babin, V.; Baucom, J.; Darden, T. A.; Sagui, C. Molecular Dynamics Simulations of DNA with Polarizable Force Fields: Convergence of an Ideal B-DNA Structure to the Crystallographic Structure. *J. Phys. Chem. B* **2006**, *110*, 11571−11581.

(6) Savelyev, A.; MacKerell, A. D. All-Atom Polarizable Force Field for DNA Based on the Classical Drude Oscillator Model. *J. Comput. Chem.* **2014**, *35*, 1219−1239.

(7) Savelyev, A.; MacKerell, A. D. Balancing the Interactions of Ions, Water, and DNA in the Drude Polarizable Force Field. *J. Phys. Chem. B* **2014**, *118*, 6742−6757.

(8) Chen, S. W.; Honig, B. Monovalent and Divalent Salt Effects on Electrostatic Free Energies Defined by the Nonlinear Poisson−Boltzmann Equation: Application to DNA Binding Reactions. *J. Phys. Chem. B* **1997**, *101*, 9113−9118.

(9) Manning, G. S. Limiting Laws and Counterion Condensation in Polyelectrolyte Solutions. III. An Analysis Based on the Mayer Ionic Solution Theory. *J. Chem. Phys.* **1969**, *51*, 3249−3252.

(10) Hayes, R. L.; Noel, J. K.; Mohanty, U.; Whitford, P. C.; Hennelly, S. P.; Onuchic, J. N.; Sanbonmatsu, K. Y. Magnesium Fluctuations Modulate RNA Dynamics in the SAM-I Riboswitch. *J. Am. Chem. Soc.* **2012**, *134*, 12043−12053.

(11) Hayes, R. L.; Noel, J. K.; Whitford, P. C.; Mohanty, U.; Sanbonmatsu, K. Y.; Onuchic, J. N. Reduced Model Captures Mg2+-RNA Interaction Free Energy of Riboswitches. *Biophys. J.* **2014**, *106*, 1508−1519.

(12) Saxena, A.; Sept, D. Multisite Ion Models That Improve Coordination and Free Energy Calculations in Molecular Dynamics Simulations. *J. Chem. Theory Comput.* **2013**, *9*, 3538−3542.

(13) Oelschlaeger, P.; Klahn, M.; Beard, W. A.; Wilson, S. H.; Warshel, A. Magnesium-Cationic Dummy Atom Molecules Enhance Representation of DNA Polymerase Beta in Molecular Dynamics Simulations: Improved Accuracy in Studies of Structural Features and Mutational Effects. *J. Mol. Biol.* **2007**, *366*, 687−701.

(14) Allnér, O.; Nilsson, L.; Villa, A. Magnesium Ion−Water Coordination and Exchange in Biomolecular Simulations. *J. Chem. Theory Comput.* **2012**, *8*, 1493−1502.

(15) Li, P.; Roberts, B. P.; Chakravorty, D. K.; Merz, K. M. Rational Design of Particle Mesh Ewald Compatible Lennard-Jones Parameters for + 2 Metal Cations in Explicit Solvent. *J. Chem. Theory Comput.* **2013**, *9*, 2733−2748.

(16) Aqvist, J. *J. Phys. Chem.* **1990**, *94*, 8021−8024.

(17) Li, P.; Merz, K. M. Taking into Account the Ion-Induced Dipole Interaction in the Nonbonded Model of Ions. *J. Chem. Theory Comput.* **2014**, *10*, 289−297.

(18) Panteva, M. T.; Giambaşu, G. M.; York, D. M. Comparison of Structural, Thermodynamic, Kinetic and Mass Transport Properties of Mg(2+) Ion Models Commonly Used in Biomolecular Simulations. *J. Comput. Chem.* **2015**, *36*, 970−982.

(19) Panteva, M. T.; Giambaşu, G. M.; York, D. M. Force Field for Mg^{2+}, Mn^{2+}, Zn^{2+}, and Cd^{2+} Ions That Have Balanced Interactions with Nucleic Acids. *J. Phys. Chem. B* **2015**, *119*, 15460−15470.

(20) Joung, I. S.; Cheatham, T. E., III. Determination of Alkali and Halide Monovalent Ion Parameters for Use in Explicitly Solvated Biomolecular Simulations. *J. Phys. Chem. B* **2008**, *112*, 9020−9041.

(21) Campbell, D. O.; Legault, P. Nuclear Magnetic Resonance Structure of the Varkud Satellite Ribozyme Stem-Loop V RNA and Magnesium-Ion Binding from Chemical-Shift Mapping. *Biochemistry* **2005**, *44*, 4157−4170.

(22) Campbell, D. O.; Bouchard, P.; Desjardins, G.; Legault, P. NMR Structure of Varkud Satellite Ribozyme Stem-Loop V in the Presence of Magnesium Ions and Localization of Metal-Binding Sites. *Biochemistry* **2006**, *45*, 10591−10605.

(23) Bergonzo, C.; Hall, K. B.; Cheatham, T. E. Stem-Loop V of Varkud Satellite RNA Exhibits Characteristics of the Mg(2+) Bound Structure in the Presence of Monovalent Ions. *J. Phys. Chem. B* **2015**, *119*, 12355−12364.

(24) Jorgensen, W. L.; Chandrasekhar, J.; Madura, J. D.; Impey, R. W.; Klein, M. L. Comparison of Simple Potential Functions for Simulating Liquid Water. *J. Chem. Phys.* **1983**, *79*, 926−935.

(25) Case, D. A.; Darden, T. A.; Cheatham, T. E., III; Simmerling, C. L.; Roitberg, A.; Wang, J.; Duke, R. E.; Luo, R.; Roe, D. R.; Walker, R. C.; Legrand, S.; Swails, J.; Cerutti, D.; Kaus, J.; Betz, R.; Wolf, R. M.; Merz, K. M.; Seabra, G.; Janowski, P.; Götz, A. W.; Kolossváry, I.; Paesani, F.; Liu, J.; Wu, X.; Steinbrecher, T.; Gohlke, H.; Homeyer, N.; Cai, Q.; Smith, W.; Mathews, D.; Salomon-Ferrer, R.; Sagui, C.; Babin, V.; Luchko, T.; Gusarov, S.; Kovalenko, A.; Berryman, J.; Kollman, P. A. *AMBER 14*; University of California: San Francisco, CA, USA, 2014.

(26) Götz, A. W.; Williamson, M. J.; Xu, D.; Poole, D.; Le Grand, S.; Walker, R. C. Routine Microsecond Molecular Dynamics Simulations with AMBER on GPUs. 1. Generalized Born. *J. Chem. Theory Comput.* **2012**, *8*, 1542−1555.

(27) Cheatham, T. E., 3rd; Cieplak, P.; Kollman, P. A. A Modified Version of the Cornell et Al. Force Field with Improved Sugar Pucker Phases and Helical Repeat. *J. Biomol. Struct. Dyn.* **1999**, *16*, 845−862.

(28) Pérez, A.; Marchán, I.; Svozil, D.; Sponer, J.; Cheatham, T. E., 3rd; Laughton, C. A.; Orozco, M. Refinement of the AMBER Force Field for Nucleic Acids: Improving the Description of Alpha/gamma Conformers. *Biophys. J.* **2007**, *92*, 3817−3829.

(29) Zgarbová, M.; Otyepka, M.; Šponer, J.; Mládek, A.; Banáš, P.; Cheatham, T. E., 3rd; Jurečka, P. Refinement of the Cornell et Al. Nucleic Acids Force Field Based on Reference Quantum Chemical Calculations of Glycosidic Torsion Profiles. *J. Chem. Theory Comput.* **2011**, *7*, 2886−2902.
(30) Essmann, U.; Perera, L.; Berkowitz, M. L.; Darden, T.; Lee, H.; Pedersen, L. G. A Smooth Particle Mesh Ewald Method. *J. Chem. Phys.* **1995**, *103*, 31−34.
(31) Ryckaert, J.-P.; Ciccotti, G.; Berendsen, H. J. C. Numerical Integration of the Cartesian Equations of Motion of a System with Constraints: Molecular Dynamics of N-Alkanes. *J. Comput. Phys.* **1977**, *23*, 327−341.
(32) Hopkins, C. W.; Le Grand, S.; Walker, R. C.; Roitberg, A. E. Long Time Step Molecular Dynamics through Hydrogen Mass Repartitioning. *J. Chem. Theory Comput.* **2015**, *11*, 1864−1874.
(33) Berendsen, H. J. C.; Postma, J. P. M.; van Gunsteren, W. F.; DiNola, A.; Haak, J. R. Molecular Dynamics with Coupling to an External Bath. *J. Chem. Phys.* **1984**, *81*, 3684−3690.
(34) Loncharich, R. J.; Brooks, B. R.; Pastor, R. W. Langevin Dynamics of Peptides: The Frictional Dependence of Isomerization Rates of N-Acetylalanyl-N′-methylamide. *Biopolymers* **1992**, *32*, 523−535.
(35) Sindhikara, D. J.; Kim, S.; Voter, A. F.; Roitberg, A. E. Bad Seeds Sprout Perilous Dynamics: Stochastic Thermostat Induced Trajectory Synchronization in Biomolecules. *J. Chem. Theory Comput.* **2009**, *5*, 1624−1631.
(36) Roe, D. R.; Cheatham, T. E., 3rd PTRAJ and CPPTRAJ: Software for Processing and Analysis of Molecular Dynamics Trajectory Data. *J. Chem. Theory Comput.* **2013**, *9*, 3084−3095.
(37) Humphrey, W.; Dalke, A.; Schulten, K. VMD: Visual Molecular Dynamics. *J. Mol. Graphics* **1996**, *14*, 33−38.
(38) Bergonzo, C.; Henriksen, N. M.; Roe, D. R.; Swails, J. M.; Roitberg, A. E.; Cheatham, T. E., 3rd Multidimensional Replica Exchange Molecular Dynamics Yields a Converged Ensemble of an RNA Tetranucleotide. *J. Chem. Theory Comput.* **2014**, *10*, 492−499.
(39) Henriksen, N. M.; Roe, D. R.; Cheatham, T. E., 3rd Reliable Oligonucleotide Conformational Ensemble Generation in Explicit Solvent for Force Field Assessment Using Reservoir Replica Exchange Molecular Dynamics Simulations. *J. Phys. Chem. B* **2013**, *117*, 4014−4027.
(40) Roe, D. R.; Bergonzo, C.; Cheatham, T. E., 3rd Evaluation of Enhanced Sampling Provided by Accelerated Molecular Dynamics with Hamiltonian Replica Exchange Methods. *J. Phys. Chem. B* **2014**, *118*, 3543−3552.

DOI: 10.1021/acs.jctc.6b00173
J. Chem. Theory Comput. 2016, 12, 3382−3389